PNAS
www.pnas.org

Supplementary Information for

The niobium and tantalum concentration in the mantle constrains the composition of Earth's primordial magma ocean

Dongyang Huang[a,1], James Badro[a], Julien Siebert[a,b]

[a]Institut de Physique du Globe de Paris, Sorbonne Paris Cité, 75005 Paris, France; [b]Institut Universitaire de France, France

[1]To whom correspondence should be addressed.

Email: huang@ipgp.fr

This PDF file includes:

Supplementary text
Figure S1-S5
Tables S1 to S3
Legend for Dataset S1-S2
SI References

Other supplementary materials for this manuscript include the following:

Dataset S1
Dataset S2

Supplementary Information Text

Synthesis of starting materials

Silicate glass: High purity oxides (MgO, Al_2O_3, and SiO_2, with or without NiO) and carbonate ($CaCO_3$) doped with Nb, Ta (sometimes with Cr and V, added as ICP standard solutions) were ground in ethanol in an agate mortar and then decarbonated, compressed and transformed into a glass in an Argon flux using aerodynamic levitation furnace coupled with 120 W CO_2 laser.

Starting metal: The piston-cylinder experiment was performed at 2 GPa and 1800 °C in a MgO capsule with graphite furnace and $BaCO_3$ cell assembly. Natural MORB was ground and mixed with high purity oxides (NiO and Cr_2O_3) and ICP vanadium standard solutions and fired at 950 °C overnight and then mixed and equilibrated with silicon-bearing iron alloy under high P-T for 2 minutes. Chemical homogeneity for both silicate and metal was confirmed by EPMA analysis, as reported in Table S2.

Sample recovery and analyses

After quench and decompression, thin sections were extracted from the center of the laser-heated area using a Ga^+ focused ion beam (FIB) instrument equipped with a field emission gun (Zeiss Auriga 40) at IPGP. Both secondary and backscattered electron images were used to monitor the sectioning. To avoid any possible contamination from adjacent phases in EDX or EPMA analysis, samples were sectioned down to 3-4 µm thick with the same geometry on both sides. Thin sections were removed from the center of the laser-heated spot by an in situ micromanipulator, and then welded to TEM copper grids with carbon deposit for further polishing and metalized for later analysis. An image of the recovered DAC sample is shown as an example in Fig. 1.

Chemical analysis of both metal and silicate phases was performed using electron probe micro-analysis (EPMA) on a Cameca SX-five at Camparis. An accelerating voltage of 15 kV and a beam current of 40 nA were used in all cases. Peak and background counting times were 15 s for major elements (Mg, Al, Ca, Fe and Si) in the silicate melts and for Fe in the quenched metals, and 60 s for minor and trace elements (Ta, Nb, Ni, V, and Cr) in both silicate and metallic phases, including Si, O, Mg, and Al in the metal, given that the detection limits were 100-400 ppm for most elements, except for Ni, Cr, V, Nb and Ta, who were more likely to be detected above 400 ppm. Diopside (Ca and Mg), orthoclase (Al and Si), hematite (Fe and O), vanadinite (V), NiO for Ni, Cr_2O_3 (Cr), and pure Nb, Ta metals were employed as internal standards. Nb was analyzed using $L_{\alpha 1}$ line, Ta using M_{α} line whereas all other elements using $K_{\alpha 1}$ line. Special care was taken to avoid analytical contamination: when the size of quenched silicate or metallic melts was comparable to the interaction volume, small beam (< 1 µm) was used and the analyzed spots were chosen far enough from the metal-silicate interface to avoid any secondary fluorescence from adjacent phases. For each phase in an individual run, 5-7 spots/windows were measured by microprobe.

Quantitative analysis was also conducted using energy dispersive X-ray (EDX) spectroscopy on FEG-FIB at IPGP. Excellent agreement was achieved for both techniques except for run X16, which has a strong fluorescence effect from surrounding silicate when analyzing the metal with EPMA, due to the large beam relative to the metal. For this reason, we opt for EDX analysis only for run X16. Accuracy of the measurements is expected to be 1 % based on the analytical calibrants.

Oxidation states of Nb and Ta in silicate melt

It has been shown by XANES measurements that Nb and Ta are pentavalent (5+) in silicate melts in moderately reducing conditions (fO_2 higher than IW-4) (1, 2). With our experiments being performed in this range of fO_2 (from IW-1 to -2, Table S1), it is reasonable to assume that Nb and Ta should remain in the 5+.

However, the valence state of a cation in silicate melt can also be determined by plotting the partition coefficient logD as a function of fO_2, at a given P and T, which must show a slope of -n/4 where n is the cation's valence. We plotted logD vs. log fO_2 in Fig. S1. We used all available experimental data (published and our data) at an fO_2 higher than IW-4. We found that the valence of Nb is 4.6 +/- 0.3 and that of Ta is 4.9 +/- 0.3. Rounded to the nearest integer, this confirms that both those elements remain pentavalent up to 94 GPa and 4500 K.

The oxygen fugacity relative to the iron-wüstite (IW) buffer is:

$$log\ fO_2 = 2\ log\left(\frac{a_{FeO}^{sil}}{a_{Fe}^{met}}\right), \qquad (S1)$$

where a_{FeO}^{sil} and a_{Fe}^{met} are the activities of FeO and Fe in the silicate and metal. This allows to express the partition coefficient explicitly as a function of fO_2 by rearranging Eq. 2 (the equilibrium constant) as:

$$log\ D\ (M) = -\frac{n}{4} log\ fO_2 + a + \frac{b}{T} + \frac{c \cdot P}{T} + d \cdot \left(\frac{nbo}{t} - 2.7\right) - log\ \gamma_M^{metal} \qquad (S2)$$

This can be rewritten as:

$$logD^*(M) = log\ D\ (M) - \frac{b}{T} - \frac{c \cdot P}{T} - d \cdot \left(\frac{nbo}{t} - 2.7\right) + log\ \gamma_M^{metal} = a - \frac{n}{4} log\ fO_2 \qquad (S3)$$

where D* is basically the partition coefficient corrected for P, T, and activity dependence. The calculations of Eq. S3 were based on measurements (Dataset S1) and parameters tabulated in Table 1. The valence state can then be obtained from the slope of logD* vs. log fO_2 in Fig. S1. Ordinary least square (OLS) regression yields n = 4.6 +/- 0.3, R^2 = 0.83 for Nb; and n = 4.9 +/- 0.3, R^2 = 0.83 for Ta. Rounded to the nearest integer, and fully consistent with all previous data, we used 5+ for both cations. Note that the valence fit is identical within uncertainties ***with*** and ***without*** our DAC data, as is shown here:

Valence Fit	Nb	Ta
Literature + This work	4.6(3)+	4.9(3)+
Literature data	4.7(3)+	5.0(3)+

Activity model for metal

To model the interactions in the metal and to correct the effects of the alloy composition on partitioning, we used the thermodynamically consistent interaction parameter (ε) approach proposed by (3), to calculate the activity coefficients of γ_{Fe} and γ_i, which has become standard practice (4–8). Following the method, the activity coefficients of the solvent (Fe) and N-1 solutes (i) for N components metallic solutions can be expressed as:

$$\ln\gamma_{Fe} = \sum_{i=1}^{N-1} \varepsilon_i^i (X_i + \ln(1-X_i)) - \sum_{j=1}^{N-2}\sum_{k=j+1}^{N-1} \varepsilon_j^k X_j X_k \left(1 + \frac{\ln(1-X_j)}{X_j} + \frac{\ln(1-X_k)}{X_k}\right)$$
$$+ \sum_{i=1}^{N-1}\sum_{\substack{k=1 \\ (k\neq i)}}^{N-1} \varepsilon_i^k X_i X_k \left(1 + \frac{\ln(1-X_k)}{X_k} - \frac{1}{1-X_i}\right) + \frac{1}{2}\sum_{j=1}^{N-2}\sum_{k=j+1}^{N-1} \varepsilon_j^k X_j^2 X_k^2 \left(\frac{1}{1-X_j} + \frac{1}{1-X_k} - 1\right) \quad (S4)$$
$$- \sum_{i=1}^{N-1}\sum_{\substack{k=1 \\ (k\neq i)}}^{N-1} \varepsilon_i^k X_i^2 X_k^2 \left(\frac{1}{1-X_i} + \frac{1}{1-X_k} + \frac{X_i}{2(1-X_i)^2} - 1\right)$$

and

$$\ln\gamma_i = \ln\gamma_{Fe} + \ln\gamma_i^0 - \varepsilon_i^i \ln(1-X_i) - \sum_{j=1(j\neq i)}^{N-1} \varepsilon_i^j X_j \left(1 + \frac{\ln(1-X_j)}{X_j} - \frac{1}{1-X_i}\right)$$
$$+ \sum_{j=1(j\neq i)}^{N-1} \varepsilon_i^j X_j^2 X_i \left(\frac{1}{1-X_i} + \frac{1}{1-X_j} + \frac{X_i}{2(1-X_i)^2} - 1\right) \quad (S5)$$

where γ_i^0 is the activity coefficient of solute i in liquid iron at infinite dilution, ε_i^j the interaction parameter of element j on element i and X_i the mole fraction of element i in the metal. Interactions between minor/trace metals are not considered, since their influence on each other are supposed to be negligible due to the low abundances. We fitted ε_i^j between light-element species (Si, O, C, and S) and minor/trace metals, including their self-interaction parameters ε_i^i, at the reference temperature 1873 K (T^0) and reported them in Table 1, together with γ_i^0 taken from *Steelmaking Data Sourcebook* (Japan Society for the Promotion of Science and the Nineteenth Committee on Steelmaking, 1988). ε_i^j and γ_i^0 were then extrapolated to run temperatures according to:

$$\ln\gamma_i^0(T) = \frac{T^0}{T}\ln\gamma_i^0(T^0) \quad (S6)$$

$$\varepsilon_i^j(T) = \frac{T^0}{T}\varepsilon_i^j(T^0) \quad (S7)$$

Following Eq. 2, the equilibrium constant K was calculated for data from literature and this study and plotted in Fig. 2.

Calculations of *nbo/t*

Following (9), *nbo* is calculated by 2*O – 4*t, where *O* is the number of oxygen atoms and *t* is the number of tetrahedral cations (including Al^{3+}, Si^{4+}, Ti^{4+}, P^{5+} and Fe^{3+}). Aluminum needs charge balance in order to be tetrahedrally coordinated, the requirement for Al^{3+} charge-compensation ($Al^{3+} < Na^{+}+K^{+}+0.5(Ca^{2+}+Mg^{2+})$) is met for all silicate composition in this study. At low oxygen fugacity conditions of our experiments almost all Fe is expected in 2+ oxidation state, therefore Fe is not considered as a possible network-forming cation occurring in tetrahedral coordination. This gives *nbo/t* values of 2 for an end member Diopside composition and 2.75 for a peridotite KLB1 composition. The calculated *nbo/t* are reported in Dataset S1.

Dependence on silicate melt composition

It has been shown that silicate melt composition, particularly the degree of polymerization which is conveniently parameterized as a function of *nbo/t*, can significantly affect the partitioning behavior between metal and silicate (10–13), especially for high valence state cations Nb and Ta. Due to the fact that the coordination environment in silicate changes from tetrahedra to octahedra at upper mantle conditions (10 to 20 GPa), the *nbo/t* calculation is no longer applicable to our higher P data (> 40 GPa),

we only calculated and fitted the *nbo/t* values for previous data less than 25 GPa and kept our *nbo/t* constant at the pyrolitic value of 2.7. The equilibrium constant K in log units is plotted as a function of *nbo/t* in Fig. S2.

The log K scatters in a range of about 2 log units even with the identical *nbo/t* values, and there is no resolvable compositional dependence regarding the degree of polymerization of silicate melt, as illustrated by the log K of Nb in Fig. S2 (open circles). This can be explained by the multiple effects of P, T and metal composition, which are not shown here and are discussed in the main manuscript. The degree of the scattering lessens and the compositional effect starts to emerge when correcting for the effects of P and T by simply subtracting the a and b terms, as can be seen from the solid circles plotted using the same dataset. In agreement with previous observations (14), Nb become more lithophile in more depolymerized melt (higher *nbo/t*), whereas pentavalent Ta is only observed to a much lesser extent. The reason, since they are not considered tetrahedral cations, may be that highly charged Nb and Ta cations require more non-bridging oxygen atoms in order to be stably incorporated in the silicate network.

Bulk *D* between Earth's core and mantle for Nb, Ni and Co

The targets (observables) to match in core formation models are the bulk partition coefficient (*D*) between Earth's core and mantle for Nb, Ni and Co, and the subchondritic Nb/Ta ratio observed in the BSE (15). The calculation of these bulk *D*s is described in detail here. Ta, on the other hand, has no target of *D* to match, in light of the well-established assumption that it is purely lithophile, which is consistent with our calculated bulk *D* for Ta close to zero (see Fig. 3 and Fig. S4).

Firstly, the concentration of an interested element in the bulk silicate Earth (x_{BSE}) is compiled from ref. (16) and ref. (17). Second, late veneer contribution is corrected assuming that the accreting materials after core formation are chondritic in its composition:

$$x_{BSE}^{LV} = \frac{f \cdot x_{BSE} - f_{LV} \cdot x_{CI}}{f - f_{LV}} \quad (S8)$$

where x_{BSE}^{LV} is the concentration in the BSE after core formation and before late veneer, f the mass fraction of the mantle in Earth which equals 0.68M_E, f_{LV} the mass fraction of the chondritic material delivered during later veneer which is estimated to be 0.005M_E, and x_{CI} the concentration in CI chondrites which is also taken from ref. (16) and ref. (17). Third, the bulk D between core and mantle after core formation can be calculated by:

$$D = \frac{(R \cdot x_{CI} - x_{BSE}^{LV}) \cdot \frac{f}{1-f}}{x_{BSE}^{LV}} \quad (S9)$$

where the numerator is the concentration of the interested element in the core. R is the average ratio of refractory lithophile elements (RLEs) concentrations or the ratio of magnesium (Mg) concentrations, between BSE and CI chondrites: for refractory elements, R equals 2.87; for elements (Ni, Co, Cr) having similar 50% condensation temperatures as Mg (T_{50} = ~1340 K) in the solar nebular, R equals 2.35. *R* is calculated from refs (17–19). $R \cdot x_{CI}$ therefore represents the content of the interested element in the BSE without any loss into the core, $(R \cdot x_{CI} - x_{BSE}^{LV}) \cdot f$ is the mass of the element sequestrated in the core, and $(R \cdot x_{CI} - x_{BSE}^{LV}) \cdot \frac{f}{1-f}$ the concentration of the interested element in the core. As can be seen in Eq. S8, the underlying assumption for this calculation is that Earth's building blocks are CI-like materials. Given $x_{BSE} = 0.595\, ppm$ and $x_{CI} = 0.283\, ppm$ with 20% and 10% uncertainties respectively, the calculated bulk $D_{\text{core-mantle}}$ for Nb equals 0.8 +/- 0.5. The calculated bulk $D_{\text{core-mantle}}$ is used as the targets in our core formation model and is listed in Dataset S2. The calculations are also performed for other carbonaceous chondrites and are reported in Dataset S2.

Effect of disequilibrium on core formation models

Our results do not address disequilibrium between the core and mantle during large impacts (e.g., Moon-forming giant impact), because such models have to assume a composition for the impactor (20, 21), which is not well constrained. Although our model does not require disequilibrium, if we assume the negative correlation between the degree of disequilibrium and Nb/Ta ratio in the BSE as in ref. (22), during late stages such giant impact would equally lower the Nb/Ta ratio in Fig. 3b, making the most reduced scenarios even less favorable, while oxidized still feasible.

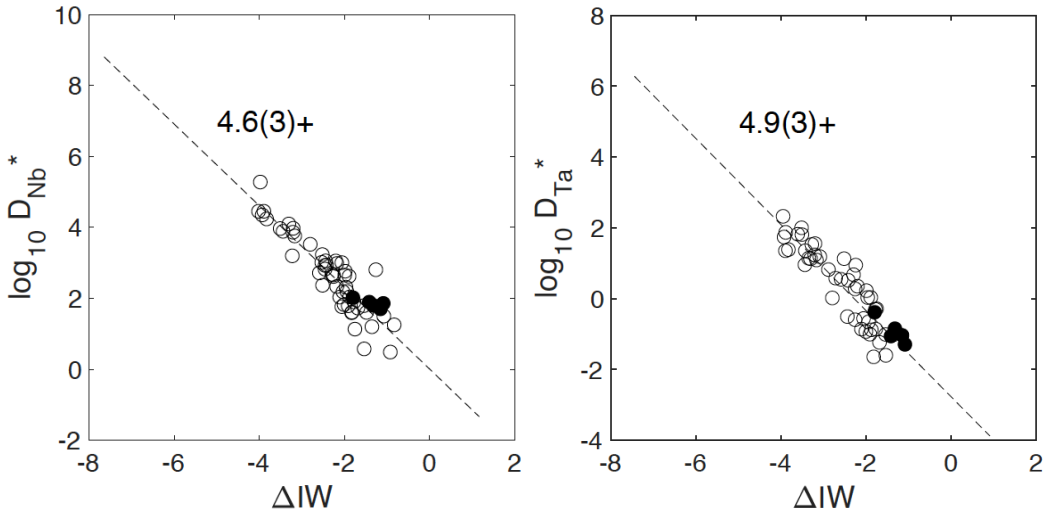

Fig. S1. Partition coefficients of Nb and Ta as a function of oxygen fugacity relative to the iron-wüstite buffer (ΔIW). Log D* denotes corrected values using Eq. S3. The regressions were performed with data collected at fO_2 above IW-4 from the literature (open circles) and our data (solid circles). The fitted oxidation states are close to 5+: 4.6+ and 4.9+ for Nb and Ta, respectively.

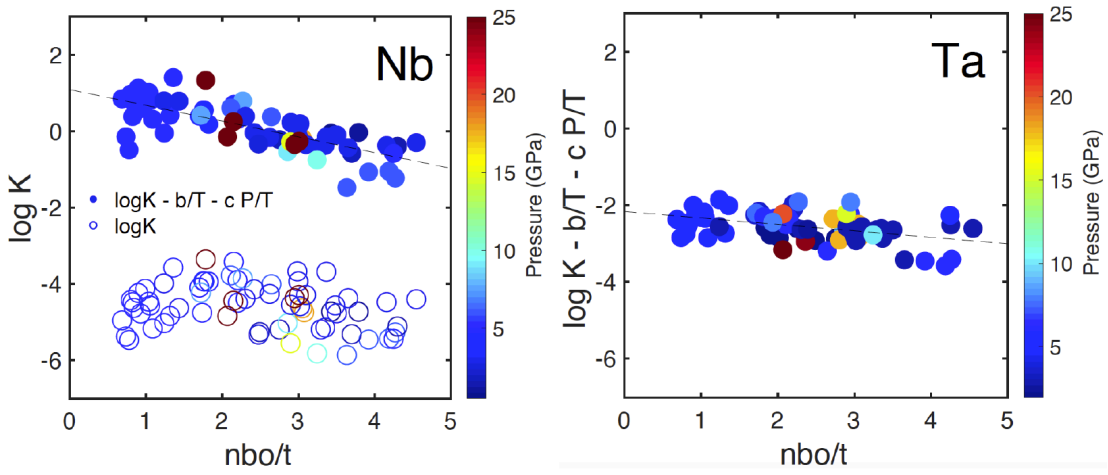

Fig. S2. Equilibrium constants (log K) for experiments conducted under 25 GPa as a function of *nbo/t* for Nb and Ta. No resolvable trend can be seen for log K of Nb (open circles), due to the combined effect of pressure and temperature. When P and T effects (*c* and *b* terms in Eq. 3) are corrected for, i.e., log K -*b*/T -*c* P/T (solid circles), Nb is found weakly dependent on the silicate melt composition, while no significant dependence is observed for Ta, consistent with ref. (14).

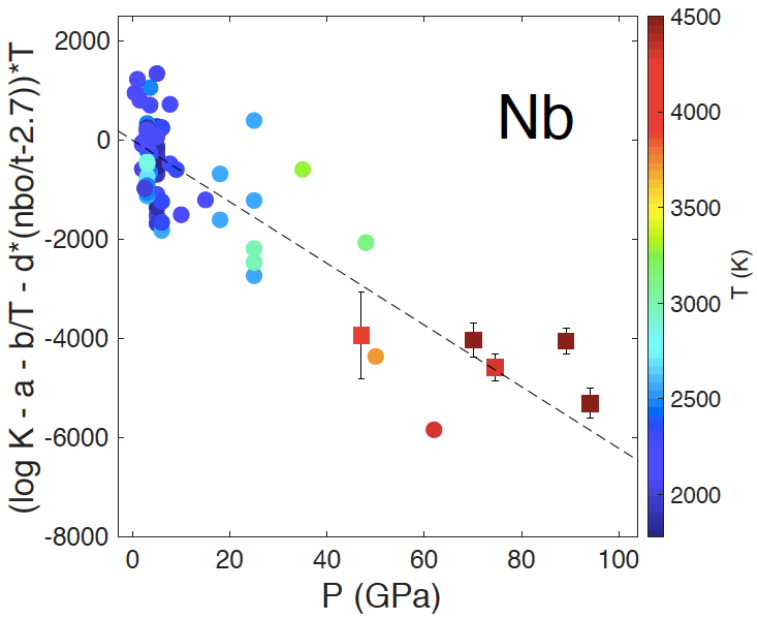

Fig. S3. Equilibrium constants (log K) for Nb as a function of pressure by correction to zero temperature and pyrolitic composition. Temperature is reported in symbol color. The dataset are the same as in Fig. 2 from (4, 7, 14, 23–27) (circles) and this study (squares). The corrected values of log K decrease with increasing pressure, i.e. Nb becomes less siderophile with pressure.

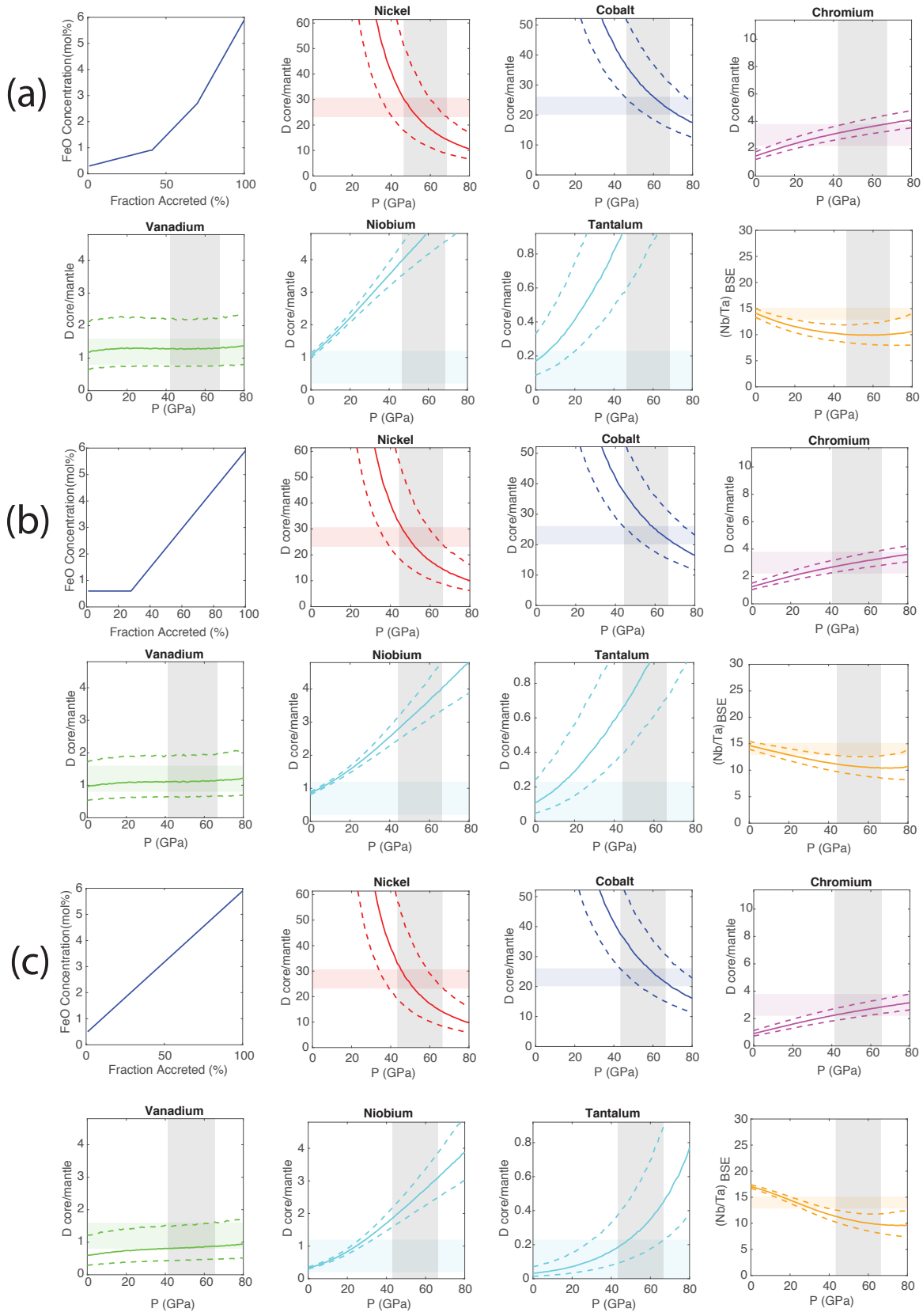
(a)
(b)
(c)
FeO Concentration(mol%)
Fraction Accreted (%)
Nickel
Cobalt
Chromium
Vanadium
Niobium
Tantalum
D core/mantle
(Nb/Ta) BSE
P (GPa)

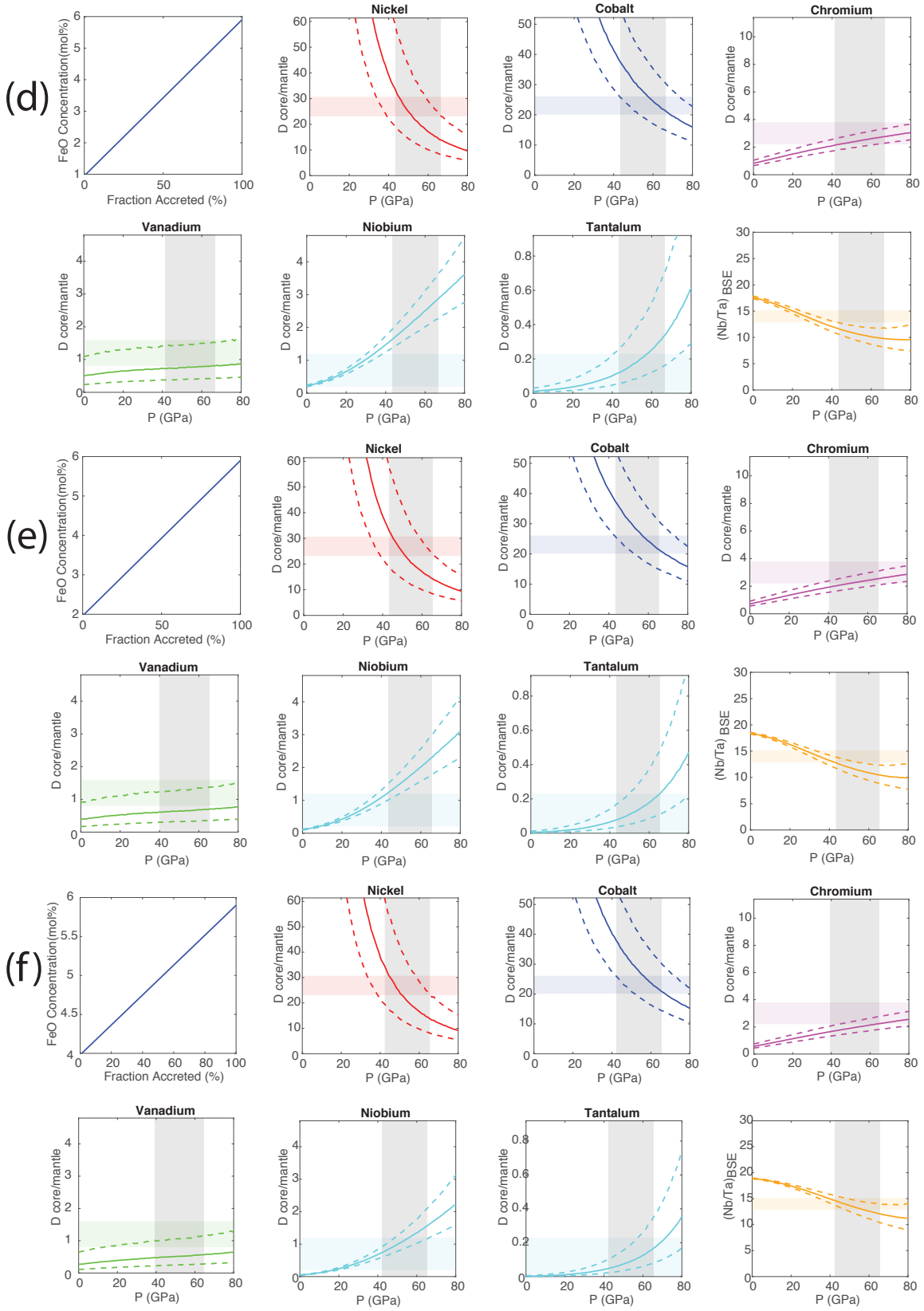
(d)
FeO Concentration(mol%)
Fraction Accreted (%)
Nickel
Cobalt
Chromium
D core/mantle
P (GPa)
Vanadium
Niobium
Tantalum
(Nb/Ta) BSE
(e)
(f)

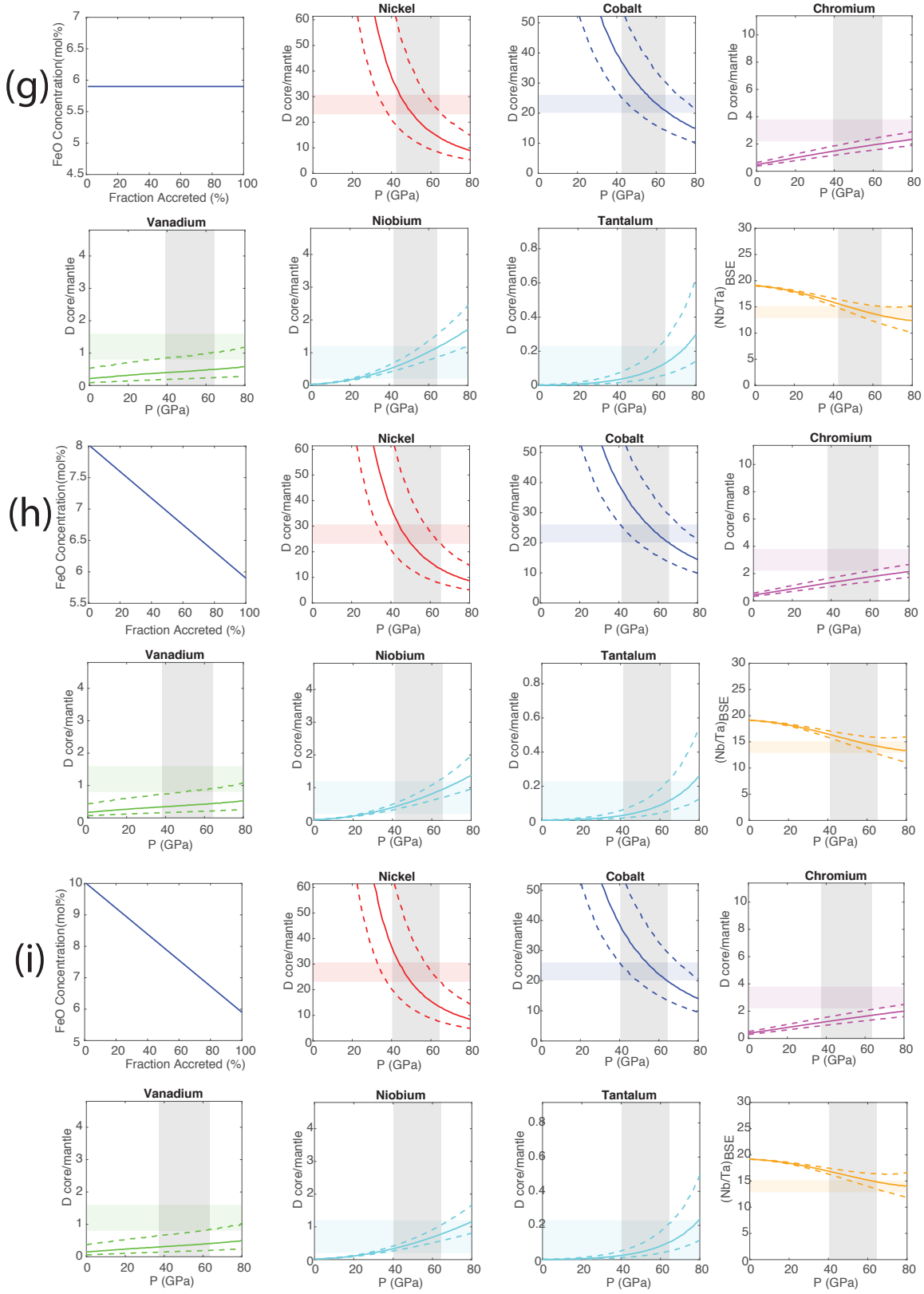
(g)
(h)
(i)
FeO Concentration(mol%)
Fraction Accreted (%)
Nickel
Cobalt
Chromium
Vanadium
Niobium
Tantalum
D core/mantle
P (GPa)
(Nb/Ta)BSE

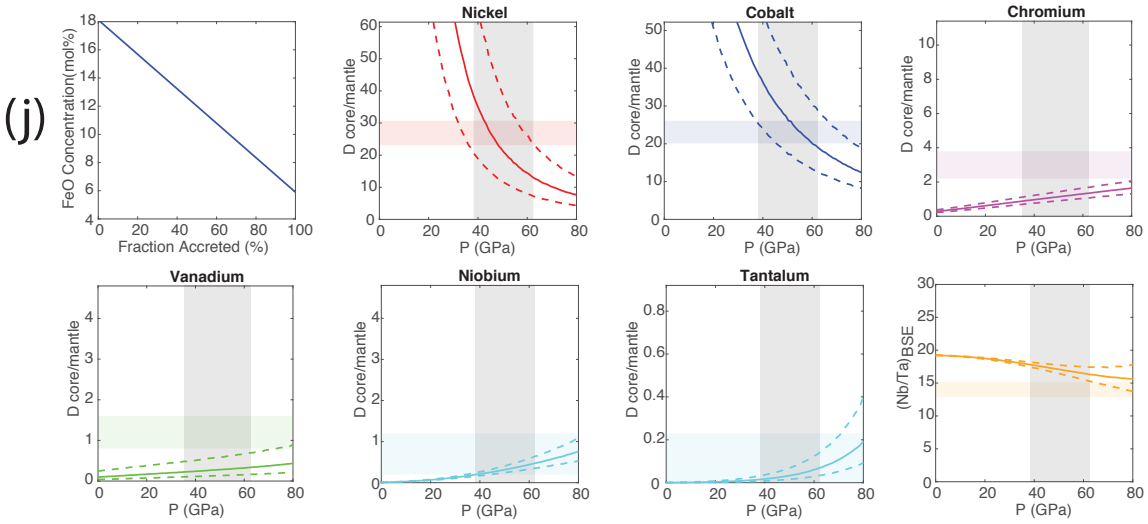

Fig. S4. Core-mantle partition coefficients of Ni, Co, Cr, V, Nb and Ta, and Nb/Ta ratio in the bulk silicate Earth (BSE) as a function of final magma ocean pressure under a range of fO_2 paths (a-j), corresponding to those of Fig. 3a. The horizontal bars correspond to the targets (present-day subchondritic Nb/Ta ratio in BSE or bulk D between core and mantle); whereas the vertical shaded area is the pressure range allowed by the observables of Ni and Co partitioning. Simultaneous match of the observables (intersections of horizontal and vertical bars) cannot be reproduced under highly reducing (a-d) nor oxidizing (h) redox conditions. The initial FeO content of Earth's magma ocean is therefore constrained to between 2 and 18 mol% (e-i).

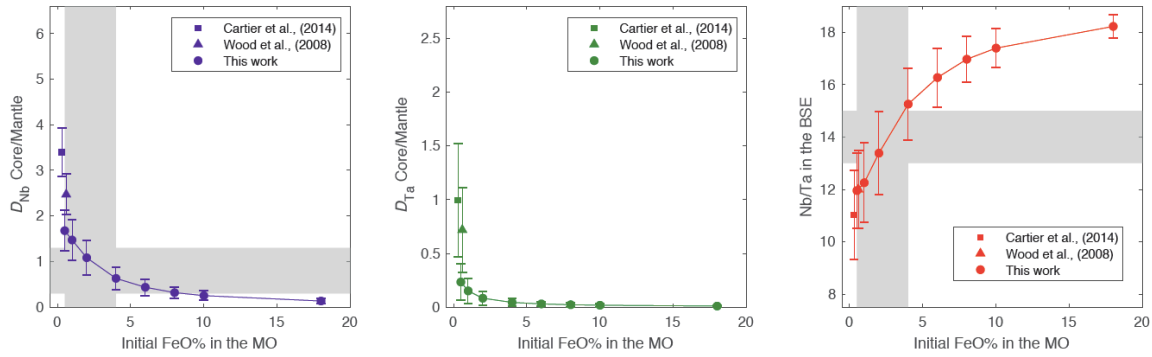

Fig. S5. Core-mantle partition coefficients of Nb (blue) and Ta (green) and Nb/Ta ratio (red) in the bulk silicate Earth (BSE) at the end of Earth's accretion, as a function of initial FeO content (in mol%) in the magma ocean (MO), ***without*** the effect of oxygen interaction. In order to test the model with low-pressure data, all the input parameters are kept the same as in Fig. 3, except that the oxygen content in the core (or ε_i^O) is set to zero (i.e., no interaction with oxygen). Without interacting with oxygen, the redox condition required to reproduce D_{Nb} and Nb/Ta in the BSE is limited to the canonical reduced conditions as shown by the vertical shaded area, which is advocated by partitioning experiments performed at relatively low pressures up to ~25 GPa (4, 23, 27, 28).

Table S1. Runs summary.

Exp. No.	X17-1	X6-1	X17-2	X9-1	X16
Pressure (GPa)	47±5	70±7	75±7	89±9	94±9
Temperature (K)	4100±200	4500±250	4300±220	4500±250	4500±250
Starting Silicate [a]	Pyrolite + Nb Ta	Pyrolite + Nb Ta	Pyrolite + Nb Ta Ni Cr V	Pyrolite + Nb Ta Ni Cr V	Pyrolite + Nb Ta Ni Cr V
Starting Metal	Fe-Si alloy (9wt% Si)	Fe-Ni alloy (by piston-cylinder)	Fe-Si alloy (9wt% Si)	Fe-Si alloy (9wt% Si)	Fe-Si alloy (9wt% Si)
fO_2 (ΔIW) [b]	-1.9	-1.5	-1.4	-1.2	-1.2

Notes:

a: All pyrolite are FeO-free.

b: Oxygen fugacity relative to the iron-wustite buffer is approximated as $fO_2(\Delta IW) = \log_{10}(xFe/xFeO)$, assuming ideal mixing.

Table S2. Starting material compositions measured by EPMA (σ corresponding to 1 standard deviations of multiple measurements).

	wt%	**σ**
Fe-Ni alloy		
O	0.22	0.02
Si	2.25	0.01
V	0.83	0.01
Cr	0.91	0.01
Fe	91.49	0.19
Ni	3.75	0.03
Total	99.45	0.19
Pyrolite + Nb Ta		
MgO	39.24	0.10
Al2O3	4.34	0.01
SiO2	50.63	0.03
CaO	2.49	0.02
Nb2O5	1.65	0.03
Ta2O5	1.26	0.06
Total	99.63	0.12
Pyrolite + Nb Ta Ni Cr V		
MgO	36.08	0.07
Al2O3	4.17	0.01
SiO2	49.38	0.02
CaO	2.32	0.01
V2O3	1.33	0.02
Cr2O3	0.32	0.01
NiO	3.45	0.02
Nb2O5	1.53	0.03
Ta2O5	1.22	0.05
Total	99.81	0.1

Table S3. EPMA results for metal and silicate (σ corresponding to 1 standard deviations of multiple measurements).

Metal

Exp. No.		N	O	Mg	Al	Si	V	Cr	Fe	Ni	Nb	Ta	Total
X16[1]	wt%	3	6.55	0.94	0.18	3.06	1.97	3.88	29.26	48.65	2.24	3.02	100.00
	σ		0.30	0.15	0.05	0.23	0.13	0.07	0.19	0.90	0.11	0.43	-
X9-1	wt%	6	5.52	0.64	0.14	4.09	2.29	4.05	31.96	38.86	3.00	0.82	91.26
	σ		0.28	0.27	0.05	0.10	0.05	0.06	0.23	0.59	0.06	0.08	0.37
X6-1	wt%	5	5.53	0.42	0.11	9.01	0.25	0.46	75.31	3.52	1.58	0.80	97.01
	σ		0.19	0.03	0.01	0.07	0.02	0.02	0.10	0.03	0.06	0.08	0.22
X17-1	wt%	5	3.52	0.46	0.06	12.28	0.00	0.00	78.43	0.00	2.40	0.60	97.80
	σ		0.37	0.33	0.01	0.34	0.00	0.00	0.62	0.00	0.05	0.12	0.64
X17-2	wt%	5	5.07	0.45	0.09	5.08	1.71	2.95	50.76	25.36	2.23	0.69	94.32
	σ		0.27	0.32	0.02	0.18	0.05	0.03	0.20	0.10	0.07	0.11	0.42

Silicate

Exp. No.		N	MgO	SiO2	CaO	FeO	NiO	Al2O3	CrO	V2O3	Nb2O5	Ta2O5	Total
X16[1]	wt%	6	26.75	28.34	2.30	8.19	9.48	5.87	3.62	4.36	5.48	5.60	100.00
	σ		0.59	0.63	0.16	0.46	0.63	0.17	0.11	0.10	0.15	0.40	-
X9-1	wt%	7	24.03	26.09	2.36	9.78	7.95	5.20	4.21	4.53	5.72	3.50	93.37
	σ		0.66	0.54	0.06	0.39	0.42	0.05	0.17	0.18	0.30	0.17	0.31
X6-1	wt%	6	32.19	35.81	2.77	18.47	0.64	6.11	0.38	0.44	1.94	1.54	100.28
	σ		1.95	1.30	0.13	1.10	0.04	0.19	0.03	0.03	0.13	0.18	2.04
X17-1	wt%	6	33.21	45.75	2.66	11.40	0.00	3.97	0.00	0.00	2.60	1.48	101.09
	σ		1.46	0.57	0.15	2.20	0.03	0.17	0.00	0.00	0.18	0.12	1.20
X17-2	wt%	5	31.31	29.83	2.64	11.46	3.47	6.19	2.77	3.32	4.03	2.91	97.93
	σ		0.53	0.43	0.05	0.56	0.33	0.15	0.03	0.06	0.20	0.13	0.54

Notes: [1]Measured by energy dispersive X-ray spectroscopy (EDX), data normalized to 100%.

Dataset S1 (separate file). Nb and Ta data employed in our thermodynamic model. Dataset includes element concentrations in Fe-rich alloys and silicate melts (in mole fraction), and *nbo/t* values.

Dataset S2 (separate file). Bulk partition coefficients between Earth's core and mantle for Ni, Co and Nb, calculated from element concentrations in the bulk silicate Earth and carbonaceous chondrites.

References

1. A. D. Burnham, A. J. Berry, B. J. Wood, G. Cibin, The oxidation states of niobium and tantalum in mantle melts. *Chem. Geol.* **330**–**331**, 228–232 (2012).
2. C. Cartier, *et al.*, Evidence for Nb 2+ and Ta 3+ in silicate melts under highly reducing conditions: A XANES study. *Am. Mineral.* **100**, 2152–2158 (2015).
3. Z. Ma, Thermodynamic description for concentrated metallic solutions using interaction parameters. *Metall. Mater. Trans. B* **32**, 87–103 (2001).
4. J. Wade, B. J. Wood, Core formation and the oxidation state of the Earth. *Earth Planet. Sci. Lett.* **236**, 78–95 (2005).
5. A. Corgne, J. Siebert, J. Badro, Oxygen as a light element: A solution to single-stage core formation. *Earth Planet. Sci. Lett.* **288**, 108–114 (2009).
6. A. Ricolleau, Y. Fei, A. Corgne, J. Siebert, J. Badro, Oxygen and silicon contents of Earth's core from high pressure metal-silicate partitioning experiments. *Earth Planet. Sci. Lett.* **310**, 409–421 (2011).
7. J. Siebert, J. Badro, D. Antonangeli, F. J. Ryerson, Terrestrial Accretion Under Oxidizing Conditions. *Science (80-.).* **339**, 1194–1197 (2013).
8. R. A. Fischer, *et al.*, High pressure metal-silicate partitioning of Ni, Co, V, Cr, Si, and O. *Geochim. Cosmochim. Acta* **167**, 177–194 (2015).
9. B. Mysen, The Structure of silicate melts. *Annu. Rev. Earth Planet. Sci.* **11**, 75–97 (1983).
10. M. J. Walter, Y. Thibault, Partitioning of tungsten and molybdenum between metallic liquid and silicate melt. *Science (80-.).* **1345**, 13–16 (1995).
11. D. Jana, D. Walker, The influence of silicate melt composition on distribution of siderophile elements among metal and silicate liquids. *Earth Planet. Sci. Lett.* **150**, 463–472 (1997).
12. H. S. C. O'Neill, S. M. Eggins, The effect of melt composition on trace element partitioning: An experimental investigation of the activity coefficients of FeO, NiO, CoO, MoO2 and MoO3 in silicate melts. *Chem. Geol.* **186**, 151–181 (2002).
13. N. L. Chabot, C. B. Agee, Core formation in the Earth and Moon: New experimental constraints from V, Cr, and Mn. *Geochim. Cosmochim. Acta* **67**, 2077–2091 (2003).
14. J. Siebert, A. Corgne, F. J. Ryerson, Systematics of metal-silicate partitioning for many siderophile elements applied to Earth's core formation. *Geochim. Cosmochim. Acta* **75**, 1451–1489 (2011).
15. C. Münker, *et al.*, Evolution of planetary cores and the Earth-Moon system from Nb/Ta systematics. *Science (80-.).* **301**, 84–87 (2003).
16. W. F. Mcdonough, S. Sun, The composition of the earth. *Chem. Geol.* **2541**, 223–253 (1995).
17. H. Palme, H. O'Neill, *Cosmochemical Estimates of Mantle Composition*, 2nd Ed. (Elsevier Ltd., 2014).
18. J. A. Barrat, *et al.*, Geochemistry of CI chondrites: Major and trace elements, and Cu and Zn Isotopes. *Geochim. Cosmochim. Acta* **83**, 79–92 (2012).
19. K. Lodders, Solar System Abundances and Condensation Temperatures of the Elements. *Astrophys. J.* **591**, 1220–1247 (2003).
20. H. Piet, J. Badro, P. Gillet, Geochemical Constraints on the Size of the Moon-Forming Giant Impact. *Geophys. Res. Lett.* **44**, 11,770-11,777 (2017).
21. J. Wade, B. J. Wood, The oxidation state and mass of the Moon-forming impactor. *Earth Planet. Sci. Lett.* **442**, 186–193 (2016).
22. C. Munker, R. O. C. Fonseca, T. Schulz, Silicate Earth's missing niobium may have been sequestered into asteroidal cores. *Nat. Geosci.* **10**, 822–826 (2017).
23. C. Cartier, T. Hammouda, M. Boyet, M. A. Bouhifd, Redox control of the fractionation of niobium and tantalum during planetary accretion and core formation. *Nat. Geosci.* **7**, 573–576 (2014).
24. A. Corgne, S. Keshav, B. J. Wood, W. F. McDonough, Y. Fei, Metal-silicate partitioning and constraints on core composition and oxygen fugacity during Earth accretion. *Geochim. Cosmochim. Acta* **72**, 574–589 (2008).
25. U. Mann, D. J. Frost, D. C. Rubie, Evidence for high-pressure core-mantle differentiation from

the metal-silicate partitioning of lithophile and weakly-siderophile elements. *Geochim. Cosmochim. Acta* **73**, 7360–7386 (2009).
26. J. Siebert, J. Badro, D. Antonangeli, F. J. Ryerson, Metal-silicate partitioning of Ni and Co in a deep magma ocean. *Earth Planet. Sci. Lett.* **321**–**322**, 189–197 (2012).
27. J. Wade, B. J. Wood, The Earth's 'missing' niobium may be in the core. *Nature* **409**, 75–78 (2001).
28. B. J. Wood, J. Wade, M. R. Kilburn, Core formation and the oxidation state of the Earth: Additional constraints from Nb, V and Cr partitioning. *Geochim. Cosmochim. Acta* **72**, 1415–1426 (2008).